IMAGE ANALYSIS TO ASSESS WOOD VARIABILITY IN LONGLEAF PINE CROSS-SECTIONAL DISKS

*Sameen Raut**

PhD Candidate
E-mail: sameen.raut@uga.edu

Joseph Dahlen†

Associate Professor
Warnell School of Forestry and Natural Resources
University of Georgia
Athens, GA 30602-2152
E-mail: jdahlen@uga.edu

(Received April 2023)

Abstract. Image analysis is an important method for rapidly measuring wood property variation, but it is infrequently applied to disks collected from forestry studies. The objective of this study was to compare image-estimated wood and bark volumes and diameters to reference measurements, and to extract more information from the images including the shape (out-of-round index, eccentric pith) and the amount and location of severe compression wood. A total of 1120 disks were cut from multiple height levels of 48 defect-free and 56 defect-containing (forking, excessive sweep, and ramicorn branching) longleaf pine (*Pinus palustris*) trees from 16 stands across Georgia (U.S.). Disks were machined on one transverse surface using a computer numeric controlled router to prepare a clean surface for imaging. Three images, one under white light, the second under blue light, and the third under blue light with a green longpass filter, were taken for each disk. Volumes and diameters estimated from images were in close agreement with reference methods. Linear models fitted as measured vs image volumes for wood and bark had coefficient of determination (R^2) values of >0.99 and 0.96. Linear models fitted as measured vs image diameters had R^2 values of >0.99. Out-of-round index and pith eccentricity values calculated from images showed a moderate positive correlation ($R = 0.43$). Algorithms developed were able to correctly identify severe compression wood, but not mild-to-moderate compression wood. Severe compression wood was moderately correlated to out-of-round index ($R = 0.54$) and pith eccentricity ($R = 0.48$). More than 98% of the disks having severe compression wood came from defect-containing trees.

Keywords: Compression wood, nondestructive evaluation, taper, wood and bark volume, wood imaging, wood and fiber quality.

INTRODUCTION

Wood is a natural heterogeneous material with properties that exhibit significant variability (Zobel and van Buijtenen 1989; Thumm et al 2010). Within a species, variability exists within annual rings, between annual rings, within trees due to changes in cardinal direction and height, between trees, between stands, and between different growing regions (Panshin and de Zeeuw 1980; Megraw 1985; Burdon et al 2004; Jordan et al 2008; Auty et al 2013, 2014; Eberhardt et al 2018). To measure variability in wood and fiber properties, typically cores are collected from trees, or disks are destructively sampled from different heights after felling (Zobel and van Buijtenen 1989; Eberhardt et al 2018). Disks are typically either processed "whole" to collect wood and bark specific gravity (SG) (density divided by the density of water) and MC, or further cut into pith-to-bark strips to provide information on radial variation (Dahlen et al 2018; Eberhardt et al 2018; Schimleck et al 2019).

Disks or bolts from felled trees can be used to assess changes in diameter from the stump (tree bottom) to the tip (tree top) to measure the stem taper (Burkhart and Tomé 2012). Outside bark diameter is typically measured using a diameter

* Corresponding author
† SWST member

tape, the inside bark diameter can be estimated using a bark gauge, or averaging two diameter measurements after felling, or from using a diameter tape following careful bark removal (Eberhardt et al 2017). These diameter measurements typically assume that the shape is circular, with tree shape evaluated qualitatively; however, research on quantitative assessment is advancing through the use of LiDAR or photogrammetric point clouds (Morgan et al 2022). In reality, disk shapes are variable, and the pith is not centered along the entire length of a tree. A major cause for eccentric radial growth is due to the formation of reaction wood, and in gymnosperms, it is termed compression wood (Timell 1986). Compression wood is generally darker in color than normal earlywood but lighter than normal latewood, and it has a high microfibril angle, high longitudinal shrinkage, high lignin content, and low cellulose content, which makes it unsuitable for lumber production and undesirable for pulp and paper (Timell 1986; Rune and Warensjö 2002).

Nondestructive evaluation of wood is increasingly being used in forestry and forest products research, operations, and manufacturing (Ross and Pellerin 1994; Ross 2015; Schimleck et al 2019). Imaging is one of many nondestructive evaluation tools which has seen extensive use (Evans 1994; Evans et al 1999; Bucur 2003a, 2003b; Decellee et al 2019; Wright et al 2019). For example, a major industrial application of imaging is in lumber manufacturing facilities, where the shape and volume of logs is measured using high-resolution laser scanners after debarking (Thomas and Bennett 2014; Sauter et al 2019). Lumber can be graded using single-pass X-ray scanners (Schajer 2001; Oh et al 2008, 2009), via the quantification of knots using the "tracheid effect", where a camera detects the returned orientation of a series of laser beams projected onto wood (Nyström 2003; Roblot et al 2010; Habite et al 2020), or using artificial intelligence (Lopes et al 2020; Hwang et al 2021; Kodytek et al 2022). Research instruments using imaging are numerous, but specific to wood and fiber quality research is the SilviScan suite of instruments that measure cell dimensions, microfibril angle, and wood density (Evans 1994; Evans et al 1999; Schimleck et al 2019). Comparatively, there are a limited number of studies conducted that describe imaging work done on whole-disks; however, this is changing due to technological advancements. In this regard, Pont et al (2007) working with radiata pine (*Pinus radiata*) disks using red-green-blue (RGB) images, delineated annual rings and detected areas of compression wood, and then created a three-dimensional (3D) stem model showing varying levels of compression wood. Thumm et al (2010) developed partial least squares regression models for near IR hyperspectral imaging data collected from radiata pine cross-sectional disks to predict and visualize variation in lignin, galactose, and glucose content. Riddell et al (2012) deployed flatbed scanning of radiata pine disks (25-35-mm thick) using transmitted light to measure spiral grain angles. Thomas and Collings (2015) used circular polarized light to enable 3D visualization of compression wood and spiral grain in microtome-cut radiata pine transverse sections. Lerm et al (2017) constructed a mobile in-field RGB imaging system and imaged cross-cut sections of *Pinus patula* logs to construct 3D models showing resin pockets, pith location, branch structure, and log shape. The DiscBot system developed by Scion was designed to measure wood property variation both radially and in circumference (Schimleck et al 2019). Raatevaara et al (2020) used RGB images of the end faces of Norway spruce (*Picea abies*) logs to extract out-of-roundness and pith eccentricity data which they combined with stem taper data to predict maximum bow height.

To calculate whole-disk SG of wood or bark, green volume is typically measured using water displacement because of the nonuniform disk shape (ASTM 2017). Imaging presents an opportunity to not only replicate the volume measurements needed for SG calculation but to further extract information from disks particularly if the surface quality is improved prior to imaging. These additional measurements could include assessments of disk shape, including how much a disk is out of round and how far the pith is from the geometric center of the disk; and the quantity and location of compression wood. An important

Table 1. Summary of the diameter outside bark (DOB) and diameter inside bark (DIB) for all the longleaf pine cross-sectional disks used in this study.

		Defect-free					Defects				
Site type	Property	N	Mean	SD	Min	Max	N	Mean	SD	Min	Max
Cutover	DOB (cm)	268	13.8	5.0	6.3	30.9	251	13.2	4.5	6.3	23.6
(*N* = 519)	DIB (cm)		12.2	4.5	5.6	28.2		11.6	3.9	5.6	20.8
Old field	DOB (cm)	277	15.5	5.8	6.6	32.5	324	14.4	5.0	6.3	27.7
(*N* = 601)	DIB (cm)		14.0	5.2	5.8	29.7		12.9	4.5	5.3	23.9
Overall	DOB (cm)	545	14.6	5.5	6.3	32.5	575	13.9	4.8	6.3	27.7
(*N* = 1120)	DIB (cm)		13.1	4.9	5.6	29.7		12.3	4.3	5.3	23.9

advantage of imaging is being able to store a digital record of the samples, as it is not typically feasible to store disks well beyond the conclusion of a study due to space considerations. Opportunities to match images with reconstructed models, to show within-tree variation with images, or even determine outliers in data due to input errors, etc. are possible with images. Hence, the objective of this study was to compare wood and bark volume information and inside and outside bark diameters with reference measurements. Additional objectives were to use the images to measure shape information including how out of round the disks are along with the pith eccentricity, and to estimate the quantity of compression wood. Images of green longleaf pine (*Pinus palustris*) disks above the FSP without any drying were collected to save measurement time and reduce cracking that occurs during the drying of disks.

MATERIALS AND METHODS

Tree Selection and Disk Extraction

Samples used for this study were collected from 16 stands of planted, unthinned longleaf pine trees throughout southern Georgia (U.S.). Stands sampled were from either cutover forest sites (where the previous rotation was trees; most likely southern pine species) or old agricultural fields (the prior rotation was not a tree species) (Hainds 2004; Johnson and Gjerstad 2006; Kush et al 2006), with eight stands sampled per site type. Stands ages ranged from 12 to 25 yr. Trees were classified as defect-free (no visible stem defects), or defect-containing (herein referred to as defect trees) ie fork, excessive sweep, or ramicorn branching present. From each stand, 20 trees were felled, with up to six defect trees sampled based on the frequency of defect trees within each stand (Raut et al 2022). From each stand, a subsample representing all of the defect trees sampled, and three defect-free trees representing a suppressed (small), codominant (medium), and dominant (large) tree were selected and used for the study for a total of 104 trees.

Cross-sectional disks (approximate thickness of 50 mm) were cut from the trees at fixed intervals: 0.15, 0.6, 1.37, and 2.44 m, and from there every 1.22 m along the tree up to the point, where the outside bark diameter was 76 mm. From the forked trees, disks were extracted from the same fixed height intervals up to the fork base before the bifurcation, from each of the fork bases after the bifurcation, and then from the height of the forks, where the outside bark diameter was 76 mm. A total of 1120 cross-sectional disks were examined, with 56 defect trees (575 disks) and 48 defect-free trees (545 disks) (Table 1). The disks were labeled, placed in plastic bags, sealed, and transported from the field to a freezer in the Wood and Fiber Quality lab at the University of Georgia, where they were kept frozen until further processing.

Disk Surfacing and Imaging

The disks were removed from the freezer and thawed for 48 h after which they were removed from their plastic bags. A three-axis computer numerical controlled (CNC) router (Fine Line Automation, Lebanon, PA) was used for machining one surface of the disks (Fig 1). The CNC

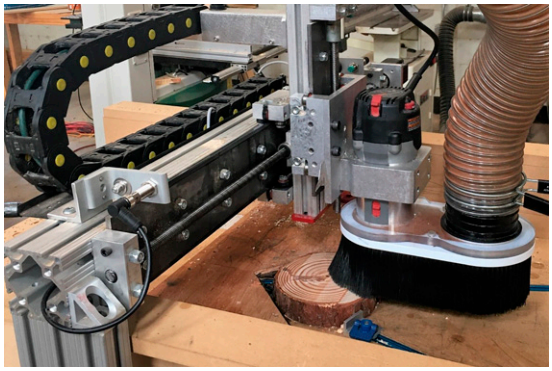

Figure 1. The three-axis computer numerical controlled (CNC) router preparing a cross-sectional disk surface for imaging.

router was controlled using an Arduino microcontroller (Arduino AG, Somerville, MA) with stepper motors used for linear motion. Since the disks were cut in the field using a chainsaw, the disk thickness varied. An ultrasonic distance sensor (Micro Detectors UK6, Modena, Italy) mounted on the *y*-axis of the CNC router was used to measure the thickness and the diameter of the disks. The disks were held on the router bed using a mechanical restraint. The router cut depth and cutting path was adjusted based on the disk thickness and diameter. The cutting bit used was an Amana Tool RC-2257 surface planer (Newton, IA). The router cut two passes on each disk, the first pass alternated the cut direction from left to right using the *y*-axis, where the router took approximately 6.4 mm off the surface of the disk (*z*-axis) in 28 mm passes (*x*-axis). The second pass skimmed the disk with 0.3 mm cut depth (*z*-axis) in 60.5 mm passes (*x*-axis). Cutting was from left to right for the second pass, and after each pass, the router returned to the left position of the *y*-axis before moving up on the *x*-axis. The second pass improved the surface for imaging (Fig 2).

Following surface preparation, images of the disks were taken using a custom-built setup with a white background and controlled using an Arduino microcontroller which interfaced with a computer running Python (Python Software Foundation, https://www.python.org/). Communication between the Arduino and Python was done using serial commands. The camera used was an Allied Vision Manta G-1236 with a 12.4-megapixel sensor (Stadtroda, Germany) and a 12 mm lens (f/2.8) (Computar, Cary, NC). The camera control was done using the Pymba library (https://github.com/morefigs/pymba). Prior to imaging, disk thickness was read by an ultrasonic sensor (Micro Detectors UK6). A linear translation stage with a stepper motor (step size = 0.0254 mm) moved the top surface of the disk to 600 mm from the camera based on the disk thickness reading from the ultrasonic sensor. Thus, each disk was imaged with a fixed focal length from the camera

Figure 2. The left image shows the typical surface quality of a chainsaw-cut wood disk; the right image shows the same disk after surface preparation (background removed from both images).

to ensure accurate calculation of diameter and area measurements.

It was found that different steps in image processing were best achieved when the disks were lit using different sources. As such, lighting for the disks was done using two LED strip light sources; white light with 4000K color temperature, and blue light (475 nm) (Super Bright LEDs Inc., St. Louis, MO). One challenge in working with images that contain both wood and bark was isolating the bark from the wood. During initial tests that were focused on using fluorescence imaging techniques with the blue LEDs and a 50-mm diameter green longpass filter (>525 nm) (Edmund Optics, Barrington, NJ) to detect compression wood (Thomas 2014), it was observed that the fluorescence image had clear separation between the bark and the wood. A total of three RGB images were taken for each machined disk. The first image was taken using white light with 12.5 ms exposure time (herein referred to as the white image). The second image was taken using blue light with 80 ms exposure time (herein referred to as the blue image). The third image was taken under blue light with 500 ms exposure time with the longpass filter moved in front of the lens using a stepper motor (herein referred to as the filter image). The three images for one disk are shown in Fig 3(a), note that the paint used to mark the location on the tree to cut disks fluoresces and appears bright orange in the filter image (this was not intended and discovered after field sampling). Images were saved with each color

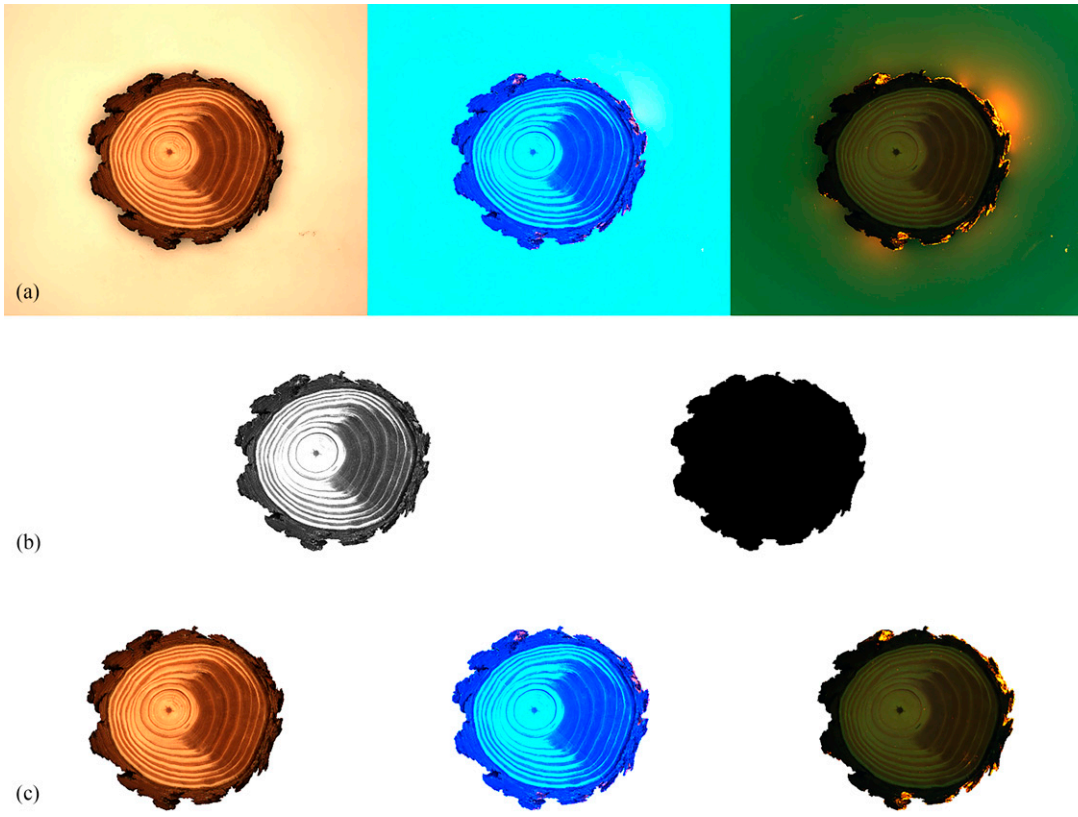

Figure 3. (a) A set of three images taken for a machined disk having a diameter outside bark (DOB) of 17.3 cm. Left: white image; middle: blue image; right: filter image. (b) Image showing the green channel of the blue image (left) and an image of the whole-disk mask (right). (c) White (left), blue (middle), and filter (right) images after the whole-disk mask was applied to the original images.

channel having an 8-bit depth, so pixel values ranged from 0 to 255 for each channel.

Disk Measurements

Following imaging, the outside bark diameters were measured to the nearest 0.1 cm with a diameter tape, and the disks were weighed to the nearest 0.01 g on a digital scale. The bark from the disks was peeled off, inside bark diameters measured, and the disks weighed again. The total bark weight for each disk was calculated from the difference in weight with and without bark. The largest piece of bark from each disk, and the peeled disks were used for volume measurement where they were labeled and submerged in water for 48-72 h. Following submerging, the bark pieces and the peeled disks were measured (separately) for their green volume to the nearest 0.01 cm^3 using water displacement (ASTM 2017). The green volume of the bark piece was then extrapolated to the total bark green volume using the total bark weight for each disk.

Image Processing

Image processing was done in Python version 3.7 (Python Software Foundation, https://www.python.org/) on the Spyder interface (Raybaut 2009) using the libraries OpenCV (Bradski 2000), NumPy (Harris et al 2020), and pandas (McKinney 2010). The camera was calibrated using various objects of known sizes and the lens was checked for distortion using OpenCV (Bradski 2000). Each pixel represented a length of 0.167 mm and an area of 0.0280 mm^2.

Background isolation. The first step in image processing was to isolate the background from the wood and the bark. The green channel of the blue image was used because the background was uniformly bright (pixel value = 255), whereas the wood and bark were darker (Fig 3[b], image on the left). A mask of the background was created by thresholding the image with any pixel less than 255 being converted to 0 (wood and bark), and any pixel equal to 255 as white (background) (Fig 3[b], image on the right). The mask from each disk was then applied to the white, blue, and filter images (Fig 3[c]).

Wood and bark isolation. After isolating the background, the location of the pith was manually determined in Python with the coordinates saved in a CSV file. The red channel of the filter image was used to isolate the bark from the wood because the inner bark near the wood and outer bark were uniformly dark and thus enabled the clear separation of wood and bark. The one area where the bark was similar to the wood was at the pith, which is made up of ground tissue, rather than the rest of the wood made up of secondary xylem tissue (Beck 2010). To isolate the pith from the bark, a white mask was applied to the pith using the coordinates of the pith (Fig 4, top left image). An initial mask of the bark was created by thresholding the image with any pixel value less than 30 being converted to 255 (white) and the rest of the pixels converted to 0 (black). The bark mask was applied on the whole-disk white images to remove the bark; however, some regions on the outside of the bark were bright due to the orange paint that fluoresced (Fig 3[a], image on the right). To correct for this, the largest contour (Arbeláez et al 2011; Papari and Petkov 2011) of the image, which was the wood, was retained and converted to a mask. A corrected bark mask (Fig 4, top right image) was created using the whole-disk mask and the wood mask. The correct bark mask was then applied to each whole-disk white image to isolate the wood from the entire disk (Fig 4, bottom left image).

Wood and bark area. The whole-disk area in pixels containing both the wood and bark was determined by counting the number of nonwhite pixels (pixel value <255) in the blue channel of the white image (Fig 3 c, image on the left). The total wood area in pixels was determined by counting the number of nonwhite pixels (pixel value <255) from the blue channel of the isolated wood image (Fig 4, bottom left image). The blue channel of the white images was used in both these instances because only the background was white (pixel value 255) and none of the disk features had a pixel value of 255. Other channels

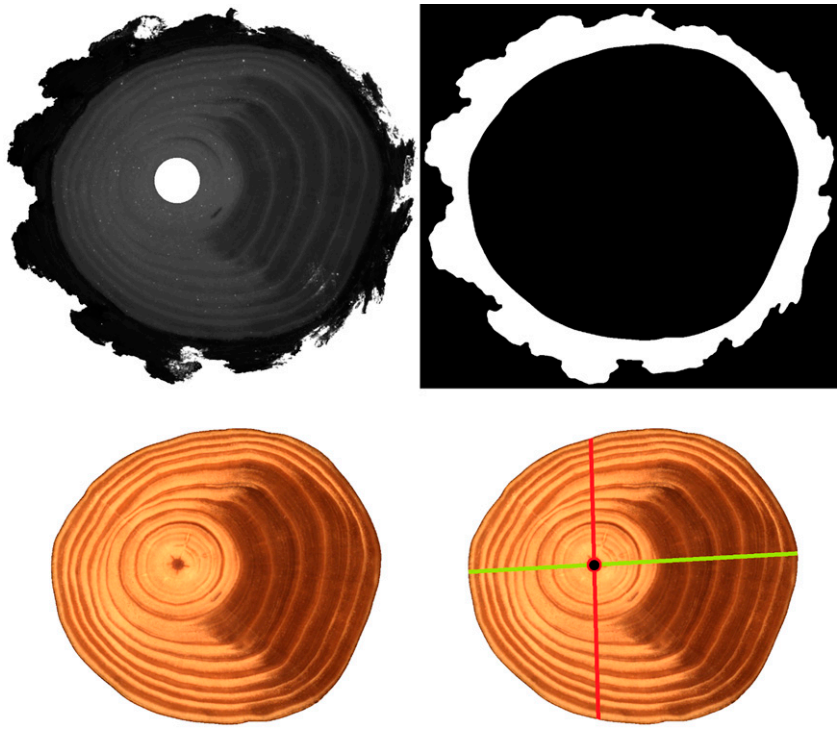

Figure 4. The top left image shows the red channel of the filter image with a white mask applied to the pith and the wood appearing lighter than the bark which appears much darker. The top right image shows the bark mask made using the whole-disk mask and the wood mask found after finding the largest contour. The bottom left image shows the isolated wood after applying the mask. The bottom right image shows the longest (green) and the shortest (red) diameters passing through the pith.

that allow whole-disk and wood area calculation in a similar fashion include the green channel of the white images, the red channel of the blue images, and all the channels (red, green, and blue) of the filter images. Hence, the red channel of the white images, and the blue and green channels of the blue images are not suitable for this purpose because earlywood in these channels appeared white (pixel value 255). The bark area was calculated by subtracting the wood area from the whole-disk area.

Inside and outside bark diameters. The whole-disk mask and the wood mask were used to detect the edges by applying a canny edge detection algorithm (Canny 1986) which returns a one-pixel-wide outline of the wood and bark edges with the edges as white (pixel value 255) and the rest of the image black (pixel value 0). To calculate the average inside and outside bark diameters, the Euclidean distance from the pith coordinates to each individual edge pixel coordinates was determined and the mean radius was calculated, which was converted to diameter. To obtain distinct edges prior to using canny edge detection, a median filter was applied to the whole-disk mask and the wood mask with a kernel (size 11×11), the images were then eroded with a kernel (size 7×7), after which they were dilated using a kernel (size 7×7) (Huang et al 1979; Efford 2000; Singh 2019).

Out-of-round index and pith eccentricity. The extent of a disk out of round was determined by calculating an index value adapted from Fallah et al (2012) which uses the maximum and the

minimum inside bark diameters in a plane that included the pith of each disk as

$$\text{Out-of-round index} = \frac{\text{Maximum diameter} - \text{Minimum diameter}}{\text{Maximum diameter}}. \quad (1)$$

To calculate the maximum and minimum inside bark diameters, all the possible straight lines passing through the pith from each individual edge pixel coordinates to their opposite ends in the canny edge image of the wood mask were determined, and then the two straight lines with the maximum and minimum length found (Fig 4, bottom right image). With Eq 1, disks that were more out of round would have an index value closer to 1 while a disk from a circular stem would have an index value closer to 0.

Pith eccentricity as defined by Moya et al (2008) was calculated as the Euclidean distance between the geometric center of the disk and the pith coordinates and is expressed as a percentage of the mean disk radius:

$$\text{Pith eccentricity } (\%) = \frac{\text{Euclidean distance between the pith and the geometric center}}{\text{Mean radius}} \times 100. \quad (2)$$

To obtain the geometric center coordinates, a contour finder algorithm on wood masks was applied which would return a single contour and then the central coordinates of the contour extracted via image moments (Bradski 2000).

Severe compression wood. To detect severe compression wood in disks, the white isolated wood images (Fig 4, bottom left image) were used and converted from RGB color space to the YCrCB color space (Jack 2007). The Cb channel (Fig 5, top left) shows the severe compression wood as being brighter than the rest of the image. The image was binarized (threshold) whereby any pixel value less than or equal to 95 (determined through experimentation) was not severe compression wood, and any pixel value greater than 95 was severe compression wood. The area near the pith was falsely classified as severe compression wood so after converting the image to binary, the pith was removed based on its coordinates. A median filter (Huang et al 1979; Singh 2019) was applied using a kernel (size 9×9) to reduce noise. The resultant compression wood mask is shown in Fig 5, top right. For the illustration of severe compression wood, the black pixels were converted to lime green (R = 153, G = 255, and B = 51) and this mask was applied to the wood images (Fig 5, bottom left). The resultant images were then manually checked to determine if the technique classified severe compression wood correctly.

The spatial distribution of severe compression wood in disks from defect trees was quantified by dividing the disks using a circular grid beginning at the pith (Fig 5, bottom right). Triangles originating from the pith were constructed at 10-degree increments with 20-pixel radius increments. At each subsection, the amount of severe compression wood as a percent of the subsection was calculated. This provided both the quantity and location of severe compression wood occurrence within a disk.

Statistical Analysis

Following the image analysis work in Python (Python Software Foundation, https://www.python.org/), the results were saved to a CSV file. For the remaining statistical analysis and graphics, R (R Core Team 2020) with the R studio interface (RStudio 2020) was used, along with the tidyverse collection of packages (Wickham et al 2019) for data munging and ggplot2 (Wickham 2016) for plotting. The length and area measurements in pixels were converted to cm or cm^2. Wood and bark areas were multiplied by the thickness of the disk (recorded using the ultrasonic sensor that positioned the disk at a fixed distance from the lens) to calculate the wood and bark volumes in cm^3. Plots were made for all volumes and diameter measurements and linear models were fitted to determine how accurate the images were to the reference measurements. The accuracy of the

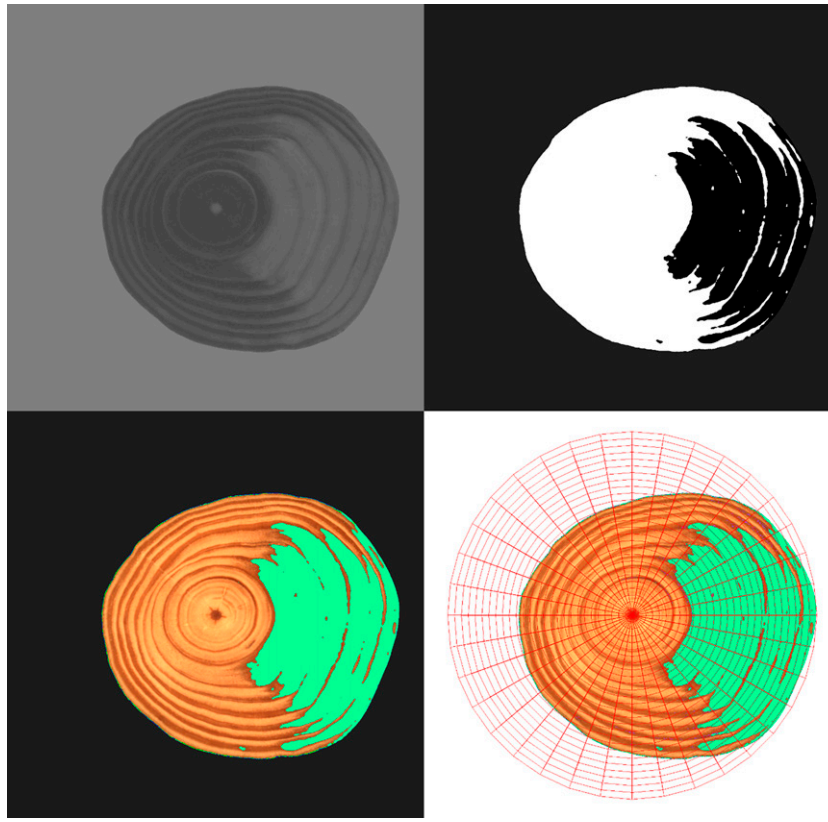

Figure 5. Steps involved in the detection and quantification of severe compression wood using the Cb channel (top left) from the YCrCb colorspace image. Image after thresholding and binarizing after removing the pith and applying a median filter (top right). The identified compression wood areas were then overlaid on wood-only images with lime green color for visualization (bottom left). A figure showing the circular grid divided into a definite number of spatially labeled subsections overlaid on to disk images from defect trees to enable quantification of severe compression wood with their location within a disk (bottom right).

image measurements was assessed by calculating the coefficient of determination (R^2) and mean absolute percentage error.

A plot showing the out-of-round index for the disks from defect and defect-free trees as a function of relative height (disk height divided by the total height) was produced. Analysis of variance (ANOVA) by means of a linear mixed effects model where stands and trees were treated as random factors was conducted using the lmerTest package (Kuznetsova et al 2017) to test for differences in out-of-round index and pith eccentricity in disks from defect and defect-free trees, and from cutover and old field sites. A plot to show the relationship between out-of-round index and pith eccentricity was created and a locally estimated scatterplot smoothing curve was fitted to the data points. Severe compression wood detection accuracy was determined qualitatively through a side-by-side visual inspection of white images with images in which severe compression wood was labeled. Spearman rank correlation was computed to indicate the strength of association between the amount of severe compression wood occurrence in a disk with out-of-round index and pith eccentricity. Quantity and location information of severe compression wood in disks from defect trees was used to create a single final map that showed the spatial distribution of severe compression wood. This was achieved in *R* using the

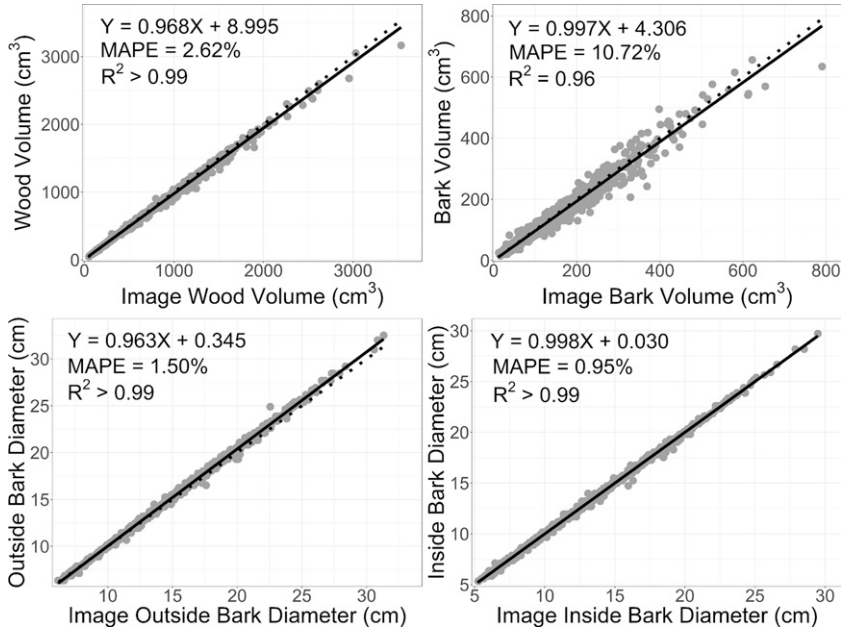

Figure 6. Reference wood and bark volumes and outside and inside bark diameter of disks plotted against the same estimates obtained from images. The solid line in each of the four plots represents the linear model fitted for the data and the dotted line represents the 1:1 line.

gstat (Pebesma 2004; Gräler et al 2016), raster (Hijmans 2022), and spatstat (Baddeley et al 2015) packages.

RESULTS

Wood and Bark Volumes and Outside Bark and Inside Bark Diameters

The relationship between the reference measurements and the image-estimated volume and diameter measurements is shown in Fig 6. The four measurements were in close agreement with the image estimated measurements. The 1:1 line (dotted line) showed that the images slightly overpredicted wood and bark volumes. The images slightly underpredicted the outside bark diameters, particularly as the diameter increased, while there was little difference between the two inside bark diameter measurements.

Out-of-Round Index and Pith Eccentricity

The mean out-of-round index value for the disks in this study was 0.06 (Table 2). The disks from defect trees had a significantly higher mean out-of-round index value (0.08) as compared with the disks from defect-free trees (0.05) ($p < 0.0001$). The first plot in Fig 7 shows that all the disks that have an out-of-round index value greater than 0.20 come from defect trees. Mean out-of-round index values for disks from cutover sites (0.07)

Table 2. Summary of out-of-round index and pith eccentricity for the overall data and separated by defect and defect-free longleaf pine trees.

	Overall				Defect-free				Defect				
Property	Mean	SD	Min	Max	Mean	SD	Min	Max	Mean	SD	Min	Max	*p* value
Out-of-round index	0.06	0.05	0.01	0.64	0.05	0.02	0.01	0.19	0.08	0.06	0.01	0.64	<0.0001
Pith eccentricity (%)	8.2	7.5	0.0	74.2	5.7	3.6	0.0	28.7	10.8	9.4	0.0	74.2	<0.0001

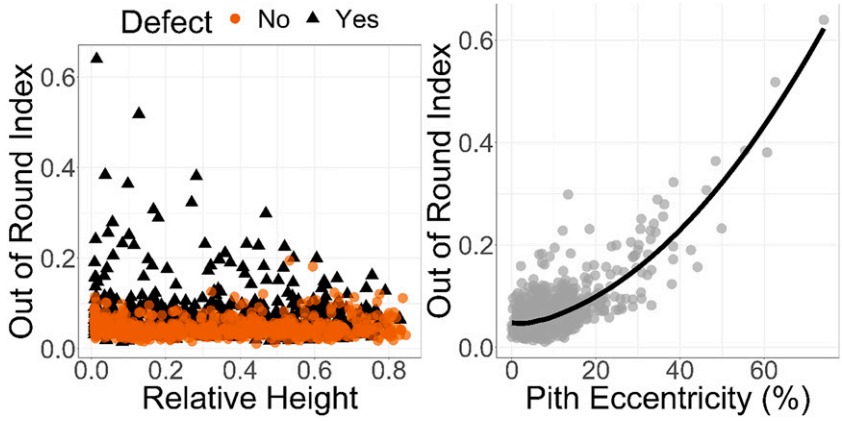

Figure 7. Out-of-round index plotted against relative height for all the disks (first plot). Out-of-round index plotted against pith eccentricity and a locally estimated scatterplot smoothing curve fitted to the data points shown in the second plot.

were not significantly different from old field sites (0.06) ($p = 0.232$). Disks that had the highest out-of-round index values (>0.3) came from relative heights less than 0.3 from defect trees (Fig 7, first plot). Disks that had the highest pith eccentricity values (>40%) came from relative heights less than 0.4 from defect trees, otherwise similar conclusions as found for out-of-round index apply here. Pith eccentricity showed a moderate positive correlation with out-of-round index ($R = 0.43$), and when plotted (Fig 7, second plot) shows a nonlinear relationship where out-of-round index increased at an increasing rate as pith eccentricity increased.

Severe Compression Wood

A total of 89 disks having severe compression wood were visually identified and the amount of severe compression wood was quantified. On disks that did not have severe compression wood (the remaining 1031 disks), latewood was falsely classified as compression wood. Hence, the algorithm is not recommended for images of disks that do not have severe compression wood or have only mild-to-moderate compression wood. In the 89 disks that had severe compression wood, on average 30.3% of the wood portion of the disks was comprised of severe compression wood (Table 3). There were 49 disks from cutover sites with 33.5% of the wood portion of the disks composed of severe compression wood, which was not significantly different from the 40 disks from old field sites that had 26.3% ($p = 0.496$). Examining the tree defect types for the 89 disks that were classified as having severe compression wood, a majority (54 out of 89) of the disks came from trees that had excessive sweep (Table 4). On average, 35.1% of the wood portion in those 54 disks from sweep trees was severe compression wood. A total of 23 disks from trees classified as having a combination of at least two or all possible visible stem defects which include forking, sweep, and ramicorn branching had severe compression wood occurrence; trees having such a combination of visible stem defects were labeled as "mixed defect" trees. There was only one disk from a tree with no visible stem defect that had

Table 3. Summary of the 89 longleaf pine disks that had severe compression wood.

	Overall ($N = 89$)				Cutover ($N = 49$)				Old field ($N = 40$)				
Property	Mean	SD	Min	Max	Mean	SD	Min	Max	Mean	SD	Min	Max	p value
Compression wood (%)	30.3	15.8	6.8	62.3	33.5	16.4	6.8	61.9	26.3	14.2	7.2	62.3	0.496
Diameter inside bark (cm)	11.2	3.5	5.8	19.8	11.1	2.9	5.8	17.8	11.2	4.2	6.1	19.8	0.831

Table 4. Summary of the 89 longleaf pine disks having severe compression wood occurrence in different defect types.

	Compression wood (%)				Out-of-round index				Pith eccentricity (%)			
Defect	Mean	SD	Min	Max	Mean	SD	Min	Max	Mean	SD	Min	Max
Fork (N = 11)	25.9	10.4	11.0	43.3	0.15	0.07	0.07	0.30	24.8	9.1	11.0	38.0
Sweep (N = 54)	35.1	16.9	6.8	62.3	0.17	0.12	0.04	0.64	26.2	15.6	4.4	74.2
Mixed defects (N = 23)	21.3	10.4	7.2	41.1	0.14	0.06	0.05	0.23	22.3	10.6	1.1	38.4
Defect-free (N = 1)	24.8	—	—	—	0.07	—	—	—	21.9	—	—	—

Mixed defects include disks from trees that had a combination of at least two visible stem defects which included forking, sweep, and ramicorn branching.

severe compression wood (Table 4). Spearman rank correlation coefficients, calculated to investigate the strength of association between out-of-round index and pith eccentricity with severe compression wood quantity, showed that both out-of-round index and pith eccentricity were moderately correlated to severe compression wood quantity with correlation coefficient values of 0.54 and 0.48, respectively. A plot showing the spatial distribution of severe compression wood occurrence relative to the disk diameter in disks from defect trees is shown in Fig 8. On average, disks from defect trees had lower severe compression wood (<1%) near the pith and the amount increased toward the bark (6%).

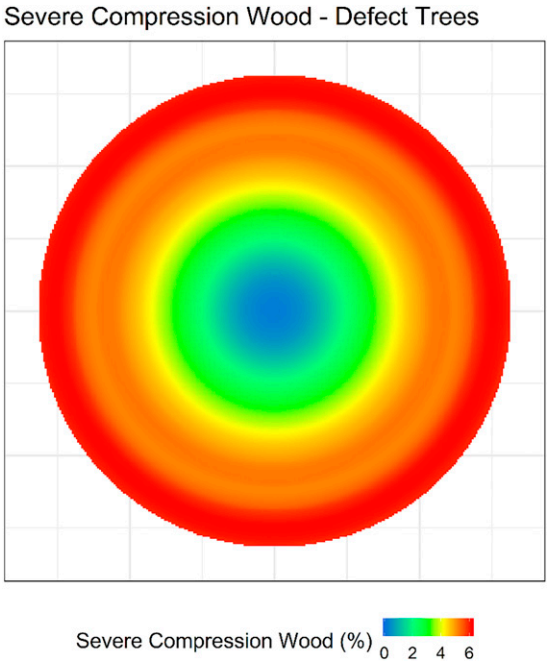

Figure 8. Spatial distribution of severe compression wood relative to the disk diameter in disks from defect trees.

DISCUSSION

It was demonstrated that imaging can be used to replicate reference measurements done on wood disks to calculate volume and diameter measurements. Overall, the volume and diameter results from the images provided similar results as the reference measurements determined using water displacement to measure volume, or using a diameter tape to measure the diameter of the disks. This was possible because of accurate camera calibration and a fixed focal length. The images slightly overpredicted the wood and bark volumes. The reason for the overprediction of wood volume is that the disk surface is assumed smooth in the images, with equal thickness throughout the entire disk. However, as only one surface was machined for imaging, the bottom surface was still rough cut from the chainsaw. This uneven surface on the bottom of the disk resulted in a slight overprediction of volume. Another reason for possible differences at the individual disk level is that images are two-dimensional, and the area calculated is for the one surface that is imaged, and thus the imaging ignores diameter changes with height due to taper (Burkhart and Tomé 2012). Other possible sources of error are localized growth deformations on the sides of the disks which are not accounted for during imaging. In addition to biological differences within the disks themselves is the accuracy of the ultrasonic sensor and the assumption that the disks were of even thickness. It is important to note that these errors were small and

imaging for wood volume had $R^2 > 0.99$. Another possible source of error is any error in the reference method, since no method is without error.

The bark volume had lower accuracy than the wood volume, but still high prediction accuracy ($R^2 = 0.96$). For wood volume, the volume measurement of wood and the imaging are done on the exact same piece, that is the full disk. Bark has more error because the image volume of bark was the entire bark, whereas with the reference method, the largest piece of bark was used (since bark comes off in pieces during the peeling process), and the volume of the piece is scaled up to the full bark volume based on the weight of the bark vs the weight of the piece. Because the image bark volume represents the entire bark volume, the image measurement is likely more accurate than the work done on the piece of bark.

The measurement of diameter from the images consistently underpredicted the outside bark diameter, whereas there was almost no difference in inside bark diameter measurements. After peeling the bark from the wood, the wood surface is relatively smooth and nearly free of any fissures. Whereas with the outside bark diameter, as the disks get larger, the outer bark shape is more irregular with more fissures (Eberhardt 2015). When measuring the diameter using a diameter tape, the diameter tape is pulled tight over the fissures which overestimate the diameter slightly. With smaller disks found higher up the tree, bark thickness is more uniform, and smaller differences were observed between the reference and the image measurements. In longleaf pine, the inner bark is approximately 15% of the total bark thickness at the stump height, whereas toward the top of the tree, the inner bark thickness is more than 40% of the total bark thickness (Eberhardt 2013).

Using the white light disk images, the amount of severe compression wood within the disks was estimated. It was acknowledged that it is an estimate as the technique only worked for severe compression wood. Generally, mild compression wood can be difficult to quantify (Thomas and Collings 2015). Here it was relatively easy to determine if the method was working for a disk by overlaying algorithm-detected severe compression wood onto the actual image, and manually verifying each disk for accuracy. The disks were imaged green as the compression wood in fresh disks had a darker reddish appearance which can improve accuracy in detection when using an RGB camera (Timell 1986; Nyström and Kline 2000). However, many researchers have noted the inability of an RGB camera alone to accurately detect compression wood areas (Duncker and Spiecker 2009), particularly for segmenting mild compression wood from latewood (Pont et al 2007). Latewood SG increases from pith to bark in southern pines including longleaf pine, with the latewood band of cells having lower density near the pith, and these rings can be difficult to distinguish even at higher resolution (Dahlen et al 2018). Nyström and Kline (2000) used a multivariate regression model to identify compression wood, using a color line scan camera and X-rays. They concluded that X-rays were not effective at compression wood identification; however, their multivariate regression model which focused on color information had an accuracy of more than 87% in detecting compression wood. The relatively high accuracy of compression wood identification by Nyström and Kline (2000) may be due to the surface imaged; they scanned the tangential and radial surfaces of green lumber, whereas the transverse surface of cross-sectional disks were imaged here. The amount of compression wood can be manually segmented on the disks themselves using a planimeter, or alternatively, the areas can be manually segmented using an image software, but both methods are extremely time consuming (Andersson and Walter 1995; Thomas 2014).

The fluorescence image could result in reliable separation between the latewood and the compression wood, but it was not the case. Thomas (2014) found that global values for thresholding compression wood were not successful for very juvenile radiata pine (*Pinus radiata*) (aged 1-3 yr old), and the same conclusion was reached here for longleaf pine. At an individual disk level, mild compression wood can be distinguished from latewood, and thus in the future, it may be possible to correctly identify compression wood using a machine

learning approach (Michelucci 2018; Bhuyan 2019; Singh 2019); however, labeling the compression wood is time-consuming. Duncker and Spiecker (2009) found that hyperspectral imaging had an accuracy greater than 91% in classifying severe compression wood, moderate compression wood, normal wood, and cracks in cross-sectional disks of Norway spruce (*Picea abies*). Cutting samples thin, either using a microtome, or to a few mm in thickness and using transmitted light can result in accurate quantification of compression wood, at the expense of greatly increased sample preparation (Andersson and Walter 1995; Rune and Warensjö 2002; Thomas 2014; Thomas and Collings 2015). Even though there are clear challenges with compression wood identification, the method was successful in extracting more information than is typically attained without imaging and the measurement and verification process is relatively fast.

A major advantage of imaging disks over the reference methods is that the images enable other measurements to be collected. For example, how much a disk was out of round and how far the pith was from the geometric center expressed as pith eccentricity was calculated. Rune and Warensjö (2002) calculated pith eccentricity and out-of-roundness for 6-yr-old, planted Scots pine (*Pinus sylvestris*) trees grown in Sweden and reported that pith eccentricity values were highest near the stem base, a finding that agrees with our pith eccentricity results. Eccentric radial growth and compression wood formation are often synonymous (Timell 1980). Rune and Warensjö (2002) reported a Spearman rank correlation coefficient of 0.44 between severe compression wood and pith eccentricity, similar to 0.48 that was found in this study. However, they found almost no correlation ($R = 0.06$) between out-of-roundness and severe compression wood and moderate correlations ($R = 0.36$) between out-of-roundness and pith eccentricity. Rune and Warensjö (2002) calculate out-of-roundness and pith eccentricity slightly different from this study; however, it is more probable that the different species and the age of the trees impacted the results. Some studies calculated the out-of-roundness and pith eccentricity the same way as Rune and Warensjö (2002) (Warensjö and Rune 2004; Raatevaara et al 2020) while others calculated them differently (Williamson 1975; Moya et al 2008; Medhurst et al 2011; Fallah et al 2012; Sauter et al 2019). The study objective was not to go in-depth and compare different studies on their methods to calculate out-of-round index and pith eccentricity values, but rather to show that the image analysis steps described can provide information to enable such calculations.

An additional advantage to imaging is the digital record of the image itself, which can be used for a number of purposes including comparing models generated to the actual disks, visual reference for different silvicultural treatments, as well as others. There is comparably little information available in the literature on imaging wood disks. The closest work is from Scion's DiscBot—which is a purpose-built wood quality instrument consisting of an RGB camera, a hyperspectral imaging system, an acoustic velocity scanner, and an X-ray system (Schimleck et al 2019). The DiscBot uses dry disks which are cut in half prior to drying to avoid cracking that occurs due to differential shrinkage (radial shrinkage is less than tangential shrinkage). After drying, the DiscBot system captures wood property variation both radially and circumferentially. Most wood and fiber quality studies looking at within-tree variation collect disks from multiple height levels, but from each disk, wood property variation is typically only measured radially, and hence, variation in circumference is not usually measured (Schimleck et al 2019). For example, the laboratory instruments used at the Wood and Fiber Quality laboratory at the University of Georgia are generally set up to work for radial variation and thus cannot be used on large disks. Here, using imaging on green disks, the surface of the disks is machined, imaged, and then processed as per the normal laboratory procedures. While variation due to circumference is usually ignored, Eberhardt et al (2018) found the northern side of mature longleaf pine trees growing in the southeastern United States to have higher ring SG and higher latewood proportion compared with the southern side.

Advancement in computing hardware in recent times has enabled complex image analysis to be carried out. For example, deep learning is one such modern machine learning image processing and data analysis tool that has shown considerable potential (Kamilaris and Prenafeta-Boldú 2018). Computer vision-based wood identification is a new research field in wood science where imaging in combination with machine learning techniques has been used to accurately identify various wood species (Yadav et al 2017; Hwang and Sugiyama 2021; Ravindran et al 2021, 2022a, 2022b). It has been noted that more complex, nonlinear methods such as deep learning with neural networks that use various convolutions to provide a hierarchical representation of data could provide more accurate estimates than existing, conventional methods (Raatevaara et al 2020; Hwang and Sugiyama 2021). However, one drawback of deep learning methods is the need for large datasets when training the models (Hwang and Sugiyama 2021). Perhaps in the future, deep learning methods of image classification of compression wood could result in accurate quantification of mild and moderate compression wood.

CONCLUSIONS

An imaging technique was developed to replicate reference wood and bark volume measurements typically made using water displacement. The results from image analysis were in close agreement with the results from the standard methods. Outside bark and inside bark diameters measured from images were also in close agreement with the measurements taken using a diameter tape. Imaging combined with effective surface preparation of green disks can aid in extracting accurate spatial measurements from images. Discrepancies between wood volume measurements were less than bark volume measurements because the wood volume measurement is done on whole-disks for both the standard and imaging methods; whereas the standard bark volume measurement is done only on the largest piece obtained after peeling bark from the green disk and the volume of that piece is then extrapolated to the total bark volume using the bark weight. Because the image represents the entire surface of the bark, it is possible that bark volume measurement from an image is more accurate than the reference method made using a bark piece. There was almost no difference between methods for measuring diameter inside bark, whereas outside bark diameter had more variability. The outside bark surface is usually rough with fissures whereas the inside bark surface is smooth and more consistent.

Estimates of how much a cross-sectional disk was out of shape by calculating an out-of-round index, and how far the pith was from the geometric center by calculating pith eccentricity values were made. Out-of-round index was found to have a moderate positive correlation with pith eccentricity. Disks that had the highest out-of-round index and pith eccentricity values came from lower sections of a defect tree having at least one visible stem defect. Both out-of-round index and pith eccentricity were moderately correlated to severe compression wood quantity. More than 98% of the disks that had severe compression wood occurrence came from defect trees. A majority of the disks (more than 60%) having severe compression wood came from trees that had excessive sweep. It was not possible to isolate mild-to-moderate compression wood from latewood using global parameters, thus the parameters would need to be tuned for each disk which necessitates the use of complex machine-learning algorithms. The methods developed in this study can be universally applied to cross-sectional disks from other southern pines and tree species of different age groups with slight modifications to the threshold values mentioned for segmentation.

ACKNOWLEDGMENTS

Funding for this research study was made possible by the NRCS (project code: 68-4310-17-012), the National Science Foundation (NSF) Center for Advanced Forest Systems (CAFS), and NIFA McIntire-Stennis (project 1023340). We are thankful to landowners Ben O'Conner, Chuck Fore, David Wells, Georgia Power, Heather Brasell, The Jones Center at Ichauway, Lynda Beam, Lamar Zipperer, Larry Hardy, Mark Dixon, Pete Peebles, Pete Studstill, and

Rayonier for allowing us to collect samples from their planted longleaf pine stands. We are grateful to Bryan Simmons, Thomas Harris, Mark Porter, and the Plantation Management Research Cooperative field crew members for their help with field work and sample collection.

REFERENCES

Andersson C, Walter F (1995) Classification of compression wood using digital image analysis. Forest Prod J 45:87-92.

Arbeláez P, Maire M, Fowlkes C, Malik J (2011) Contour detection and hierarchical image segmentation. IEEE Trans P Anal Mach Intell 33:898-916. https://doi.org/10.1109/TPAMI.2010.161

ASTM (2017) D2395-17. Standard test methods for density and specific gravity (relative density) of wood and wood-based materials. ASTM, West Conshohocken, PA.

Auty D, Achim A, Macdonald E, Cameron AD, Gardiner BA (2014) Models for predicting wood density variation in Scots pine. Forestry 87:449-458. https://doi.org/10.1093/forestry/cpu005

Auty D, Gardiner BA, Achim A, Moore JR, Cameron AD (2013) Models for predicting microfibril angle variation in Scots pine. Ann Sci 70:209-218. https://doi.org/10.1007/s13595-012-0248-6

Baddeley A, Rubak E, Turner R (2015) Spatial point patterns: methodology and applications with R. Chapman and Hall/CRC Press, London, UK.

Beck CB (2010) An introduction to plant structure and development: plant anatomy for the twenty-first century, 2nd edition. Cambridge University Press, Cambridge, UK.

Bhuyan MK (2019) Computer vision and image processing: fundamentals and applications. CRC Press, Boca Raton, FL.

Bradski G (2000) The OpenCV library. Dr Dobb's J Softw Tools 120:122-125.

Bucur V (2003a) Nondestructive characterization and imaging of wood. Springer, Heidelberg.

Bucur V (2003b) Techniques for high resolution imaging of wood structure: a review. Meas Sci Technol 14:R91-R98. https://doi.org/10.1088/0957-0233/14/12/R01

Burdon RD, Paul Kibblewhite R, Walker JCF, Megraw RA, Evans R, Cown DJ (2004) Juvenile versus mature wood: a new concept, orthogonal to corewood versus outerwood, with special reference to *Pinus radiata* and *P. taeda*. Forest Sci 50:399-415. https://doi.org/10.1139/x84-145

Burkhart HE, Tomé M (2012) Modeling forest trees and stands. Springer, Dordrecht, Netherlands.

Canny J (1986) A computational approach to edge detection. IEEE Trans P Anal Mach Intell PAMI-8:679-698. https://doi.org/10.1109/TPAMI.1986.4767851

Dahlen J, Auty D, Eberhardt TL (2018) Models for predicting specific gravity and ring width for loblolly pine from intensively managed plantations, and implications for wood utilization. Forests 9:1-20. https://doi.org/10.3390/f9060292

Decellee R, Ngo P, Debled-Rennesson I, Mothe F, Longuetaud F (2019) A new algorithm to automatically detect the pith on rough log-end images. Pages 518-523 *in* X Wang, UH Sauter, RJ Ross, eds. Proceedings, 21st International Nondestructive Testing and Evaluation of Wood Symposium, September 24–27, 2019. General Technical Report FPL-GTR-272. USDA Forest Service, Forest Products Laboratory, Madison, WI.

Duncker P, Spiecker H (2009) Detection and classification of Norway spruce compression wood in reflected light by means of hyperspectral image analysis. IAWA J 30:59-70. https://doi.org/10.1163/22941932-90000203

Eberhardt TL (2013) Longleaf pine inner bark and outer bark thicknesses: measurement and relevance. South J Appl For 37:177-180. https://doi.org/10.5849/sjaf.12-023

Eberhardt TL (2015) Thickness and roughness measurements for air-dried longleaf pine bark. Pages 374-379 *in* AG Holley, KF Connor, JD Haywood eds. Proceedings, 17th Biennial Southern Silvicultural Research Conference, March 5–7, 2013. e-General Technical Report SRS-203. USDA Forest Service, Southen Research Station, Asheville, NC.

Eberhardt TL, Dahlen J, Schimleck L (2017) Species comparison of the physical properties of loblolly and slash pinewood and bark. Can J Res 47:1495-1505. https://doi.org/10.1139/cjfr-2017-0091

Eberhardt TL, So CL, Leduc DJ (2018) Wood variability in mature longleaf pine: differences related to cardinal direction for a softwood in a humid subtropical climate. Wood Fiber Sci 50:1-14.

Efford N (2000) Digital image processing: a practical introduction using Java, 1st edition. Addison-Wesley Longman Publishing Co., Inc., Boston, MA.

Evans R (1994) Rapid measurement of the transverse dimensions of tracheids in radial wood sections from *Pinus radiata*. Holzforschung 48:168-172. https://doi.org/10.1515/hfsg.1994.48.2.168

Evans R, Hughes M, Menz D (1999) Microfibril angle variation by scanning X-ray diffractometry. Appita J 52:363-367.

Fallah A, Riahifar N, Barari K, Parsakhoo A (2012) Investigating the out-of-roundness and pith-off-centre in stems of three broadleaved species in Hyrcanian forests. J Sci 58:513-518. https://doi.org/10.17221/13/2012-jfs

Gräler B, Pebesma E, Heuvelink G (2016) Spatio-temporal interpolation using gstat. R J 8:204-218.

Habite T, Olsson A, Oscarsson J (2020) Automatic detection of pith location along Norway spruce timber boards on the basis of optical scanning. Eur J Wood Wood Prod 78:1061-1074. https://doi.org/10.1007/s00107-020-01558-1

Hainds MJ (2004) Establishing longleaf pine seedlings on agricultural fields and pastures. Pages 309–313 *in*

Connor KF, ed. Proceedings, 12th Biennial Southern Silvicultural Research Conference, February 24–28, 2003. General Technical Report SRS-71. USDA Forest Service, Southern Research Station, Asheville, NC.

Harris CR, Millman KJ, van der Walt SJ, Gommers R, Virtanen P, Cournapeau D, Wieser E, Taylor J, Berg S, Smith NJ, Kern R, Picus M, Hoyer S, van Kerkwijk MH, Brett M, Haldane A, Del Río JF, Wiebe M, Peterson P, Gérard-Marchant P, Sheppard K, Reddy T, Weckesser W, Abbasi H, Gohlke C, Oliphant TE (2020) Array programming with NumPy. Nature 585:357-362. https://doi.org/10.1038/s41586-020-2649-2

Hijmans RJ (2022) raster: geographic data analysis and modeling. R package version 3.5-21. https://CRAN.R-project.org/package=raster (4 April 2022).

Huang TS, Yang GJ, Tang GY (1979) A fast two-dimensional median filtering algorithm. IEEE Trans Acoust 27:13-18. https://doi.org/10.1109/TASSP.1979.1163188

Hwang SW, Lee T, Kim H, Chung H, Choi JG, Yeo H (2021) Classification of wood knots using artificial neural networks with texture and local feature-based image descriptors. Holzforschung 76:1-13. https://doi.org/10.1515/hf-2021-0051

Hwang SW, Sugiyama J (2021) Computer vision-based wood identification and its expansion and contribution potentials in wood science: a review. Plant Methods 17:47. https://doi.org/10.1186/s13007-021-00746-1

Jack K (2007) Video demystified: a handbook for the digital engineer, 5th edition. Newnes, Newton, MA.

Johnson R, Gjerstad D (2006) Restoring the overstory of longleaf pine ecosystems. Pages 271-295 *in* S Jose, EJ Jokela, DL Miller, eds. The longleaf pine ecosystem: ecology, silviculture, and restoration. Springer, New York, NY.

Jordan L, Clark A, Schimleck LR, Hall DB, Daniels RF (2008) Regional variation in wood specific gravity of planted loblolly pine in the United States. Can J Res 38:698-710. https://doi.org/10.1139/X07-158

Kamilaris A, Prenafeta-Boldú FX (2018) Deep learning in agriculture: a survey. Comput Electron Agric 147:70-90. https://doi.org/10.1016/j.compag.2018.02.016

Kodytek P, Bodzas A, Bilik P (2022) A large-scale image dataset of wood surface defects for automated vision-based quality control processes. F1000 Res 10:581. https://doi.org/10.12688/f1000research.52903.2

Kush JS, Goelz JCG, Williams RA, Carter DR, Linehan PE (2006) Longleaf pine growth and yield. Pages 251–267 *in* S Jose, EJ Jokela, DL Miller, eds. The longleaf pine ecosystem: ecology, silviculture, and restoration. Springer, New York, NY.

Kuznetsova A, Brockhoff PB, Christensen RHB (2017) lmerTest package: tests in linear mixed effects models. J Stat Softw 82:1-26. https://doi.org/10.18637/jss.v082.i13

Lerm FJ, Blumentritt M, Brink WH, Wessels CB (2017) A method for three-dimensional stem analysis and its application in a study on the occurrence of resin pockets in *Pinus patula*. Eur J For Res 136:411-420. https://doi.org/10.1007/s10342-017-1041-8

Lopes DJV, Bobadilha GDS, Grebner KM (2020) A fast and robust artificial intelligence technique for wood knot detection. BioResources 15:9351-9361. https://doi.org/10.15376/biores.15.4.9351-9361

McKinney W (2010) Data structures for statistical computing in Python. Pages 56-61 *in* Proceedings, 9th Python in Science Conference, June 28–July 3, 2010. Austin, Texas.

Medhurst J, Ottenschlaeger M, Wood M, Harwood C, Beadle C, Valencia JC (2011) Stem eccentricity, crown dry mass distribution, and longitudinal growth strain of plantation-grown *Eucalyptus nitens* after thinning. Can J Res 41:2209-2218. https://doi.org/10.1139/x11-135.

Megraw RA (1985) Wood quality factors in loblolly pine: the influence of tree age, position in tree, and cultural practice on wood specific gravity, fiber length, and fibril angle. TAPPI Press, Peachtree Corners, GA, USA.

Michelucci U (2018) Advance applied deep learning. Springer, New York, NY.

Morgan CJ, Powers M, Strimbu BM (2022) Estimating tree defects with point clouds developed from active and passive sensors. Remote Sens 14:1938. https://doi.org/10.3390/rs14081938

Moya R, Araya L, Vilchez B (2008) Variation in the pith parameter of *Gmelina arborea* trees from fast growth plantations in Costa Rica. Ann Sci 65:612-621. https://doi.org/10.1051/forest:2008045

Nyström J (2003) Automatic measurement of fiber orientation in softwoods by using the tracheid effect. Comput Electron Agric 41:91-99. https://doi.org/10.1016/S0168-1699(03)00045-0

Nyström J, Kline DE (2000) Automatic classification of compression wood in green southern yellow pine. Wood Fiber Sci 32:301-310.

Oh JK, Kim KM, Lee JJ (2008) Development of knot quantification method to predict bending strength using X-ray scanner. J Korean Wood Sci Technol 36:33-41.

Oh JK, Shim K, Kim KM, Lee JJ (2009) Quantification of knots in dimension lumber using a single-pass X-ray radiation. J Wood Sci 55:264-272. https://doi.org/10.1007/s10086-009-1031-7

Panshin AJ, de Zeeuw C (1980) Textbook of wood technology: structure, identification, properties, and uses of commercial woods of the United States and Canada, 4th edition. McGraw Hill, New York, NY.

Papari G, Petkov N (2011) Edge and line oriented contour detection: state of the art. Image Vis Comput 29:79-103. https://doi.org/10.1016/j.imavis.2010.08.009

Pebesma EJ (2004) Multivariable geostatistics in S: the gstat package. Comput Geosci 30:683-691.

Pont D, Brownlie RK, Grace JC (2007) Disc image-processing software for three-dimensional mapping of stem ring width and compression wood. N Z J For Sci 37:169-185.

R Core Team (2020) R: a language and environment for statistical computing. R Foundation for Statistical Computing, Vienna, Austria. https://www.R-project.org/ (3 April 2020).

Raatevaara A, Korpunen H, Mäkinen H, Uusitalo J (2020) Log end face image and stem tapering indicate maximum bow height on Norway spruce bottom logs. Eur J For Res 139:1079-1090. https://doi.org/10.1007/s10342-020-01309-0

Raut S, Dahlen J, Bullock B, Montes CR, Dickens D (2022) Models to predict whole-disk specific gravity and moisture content in planted longleaf pine from cutover and old field sites. Can J Res 52:137-147. https://doi.org/10.1139/cjfr-2021-0092

Ravindran P, Owens FC, Wade AC, Shmulsky R, Wiedenhoeft AC (2022a) Towards sustainable North American wood product value chains, Part I: computer vision identification of diffuse porous hardwoods. Front Plant Sci 12:758455. https://doi.org/10.3389/fpls.2021.758455

Ravindran P, Owens FC, Wade AC, Vega P, Montenegro R, Shmulsky R, Wiedenhoeft AC (2021) Field-deployable computer vision wood identification of Peruvian timbers. Front Plant Sci 12:647515. https://doi.org/10.3389/fpls.2021.647515

Ravindran P, Wade AC, Owens FC, Shmulsky R, Wiedenhoeft AC (2022b) Towards sustainable North American wood product value chains, Part 2: computer vision identification of ring-porous hardwoods. Can J Res 52:1014–1027. https://doi.org/10.1139/cjfr-2022-0077

Raybaut P (2009) Spyder-documentation. https://www.spyder-ide.org. Accessed April 4, 2020.

Riddell M, Cown D, Harrington J, Lee J, Moore J (2012) Assessing spiral grain angle by light transmission: - proof of concept -. IAWA J 33:1-14. https://doi.org/10.1163/22941932-90000075

Roblot G, Bléron L, Mériaudeau F, Marchal R (2010) Automatic computation of the knot area ratio for machine strength grading of Douglas-fir and Spruce timber. Eur J Environ Civ Eng 14:1317-1332. https://doi.org/10.3166/ejece.14.1317-1332

Ross RJ (2015) Nondestructive testing and evaluation of wood. Page 169 *in* RJ Ross ed. Nondestructive evaluation of wood, 2nd edition. General Technical Report FPL-GTR-238. USDA Forest Service, Forest Products Laboratory, Madison, WI.

Ross RJ, Pellerin RF (1994) Nondestructive testing for assessing wood members in structures: a review. General Technical Report FPL-GTR-70. USDA Forest Service, Forest Products Laboratory, Madison, WI.

RStudio (2020) RStudio: integrated development for R. RStudio, Inc., Boston, MA. http://www.rstudio.com/ (3 April 2020).

Rune G, Warensjö M (2002) Basal sweep and compression wood in young Scots pine trees. Scand J Fr Res 17:529-537. https://doi.org/10.1080/02827580260417189

Sauter UH, Staudenmaier J, Huber M (2019) High-precision determination of round wood diameters and cross-section areas. Pages 584-587 *in* X Wang, UH Sauter, RJ Ross eds. Proceedings, 21st International Nondestructive Testing and Evaluation of Wood Symposium, September 24–27, 2019. General Technical Report FPL-GTR-272. USDA Forest Service, Forest Products Laboratory, Madison, WI.

Schajer GS (2001) Lumber strength grading using X-ray scanning. Forest Prod J 51:43-52.

Schimleck L, Dahlen J, Apiolaza LA, Downes GM, Emms GW, Evans R, Moore JR, Pâques L, Van den Bulcke J, Wang X (2019) Non-destructive evaluation techniques and what they tell us about wood property variation. Forests 10:728. https://doi.org/10.3390/f10090728.

Singh H (2019) Practical machine learning and image processing. Springer, New York, NY.

Thomas J (2014) An investigation on the formation and occurrence of spiral grain and compression wood in radiata pine (*Pinus radiata* D. Don.). PhD thesis, University of Canterbury, Christchurch, New Zealand.

Thomas J, Collings DA (2015) Three-dimensional visualization of spiral grain and compression wood in Pinus radiata imaged by circular polarized light and fluorescence. Wood Fiber Sci 48:22-27.

Thomas RE, Bennett ND (2014) Accurately determining log and bark volumes of saw logs using high-resolution laser scan data. Pages 299-310 *in* JW Groninger, EJ Holzmueller, CK Nielsen, and DC Dey, eds. Proceedings, 19th Central Hardwood Forest Conference, March 10–12, 2014. GTR-NRS-P-142. USDA Forest Service, Northern Research Station, Carbondale, IL.

Thumm A, Riddell M, Nanayakkara B, Harrington J, Meder R (2010) Near infrared hyperspectral imaging applied to mapping chemical composition in wood samples. J Near Infrared Spectrosc 18:507-515. https://doi.org/10.1255/jnirs.909

Timell TE (1980) Karl Gustav Sanio and the first scientific description of compression wood. IAWA J 1:147-153.

Timell TE (1986) Compression wood in gymnosperms. Springer-Verlag, Berlin, Germany.

Warensjö M, Rune G (2004) Stem straightness and compression wood in a 22-year-old stand of container-grown Scots pine trees. Silva Fenn 38:143-153. https://doi.org/10.14214/sf.424

Wickham H (2016) ggplot2: elegant graphics for data analysis. Springer-Verlag, New York, NY.

Wickham H, Averick M, Bryan J, Chang W, McGowan LDA, François R, Grolemund G, Hayes A, Henry L, Hester J, Kuhn M, Pedersen TL, Miller E, Bache SM, Müller K, Ooms J, Robinson D, Seidel DP, Spinu V, Takahashi K, Vaughan D, Wilke C, Woo K, Yutani H (2019) Welcome to the tidyverse. J Open Source Softw 4:1686. https://doi.org/10.21105/joss.01686

Williamson RL (1975) Out-of-roundness in Douglas-fir stems. Forest Sci 21:365-370.

Wright S, Dahlen J, Montes C, Eberhardt TL (2019) Quantifying knots by image analysis and modeling their

effects on the mechanical properties of loblolly pine lumber. Eur J Wood Wood Prod 77:903-917. https://doi.org/10.1007/s00107-019-01441-8

Yadav A, Anand RS, Dewal M, Gupta S (2017) Binary wavelet transform-based completed local binary pattern texture descriptors for classification of microscopic images of hardwood species. Wood Sci Technol 51: 909-927. https://doi.org/10.1007/s00226-017-0902-0

Zobel BJ, van Buijtenen JP (1989) Wood variation: its causes and control. Springer-Verlag, Berlin, Heidelberg.